FABRICATION OF EMBEDDED HORIZONTAL MICRO-CHANNELS USING LINE-SCAN STEREOLITHOGRAPHY

Jae-Won Choi[1], Rolando Quintana[2], and Ryan B. Wicker[1]
[1]W.M. Keck Center for 3D Innovation, The University of Texas at El Paso, El Paso, TX 79968
[2]Department of Management Science and Statistics, The University of Texas at San Antonio, San Antonio, TX 78279

Reviewed, accepted September 10, 2008

ABSTRACT

In an effort to directly and rapidly manufacture micro-fluidic devices with embedded horizontal micro-channels on the order of tens of microns, a method was developed for using current commercially available line-scan stereolithography (SL) technology. The method consisted of inserting a wire of specified diameter during the build, building around the inserted wire, and removing the wire once fabricated leaving a channel with a circular cross-sectional geometry equivalent to the wire diameter. Demonstration of the technique using 31.6 μm, 57.2 μm and 83.5 μm wire was performed using a 3D Systems Viper si2™ SL system and DSM Somos® WaterShed™ resin. By embedding the wire and building around the insert, the down-facing surfaces were supported during fabrication enabling successful and accurate fabrication of embedded micro-channel geometries. A method for successful fabrication was developed that involved first building an open micro-channel, interrupting the SL process and inserting the wire, and then capping over the wire with multiple layers. After fabricating a part with a micro-wire, the micro-channel was produced by simply pulling the wire out of the part. Scanning electron microscope (SEM) images were used to examine and measure the geometries of the fabricated micro-channels, and a statistical design of experiments was performed to show that the process was capable of producing accurate horizontal micro-channels. It is expected that this process will enable unique micro-fluidic and other applications of micro-channel fabrication to be pursued using commercial line-scan SL.

INTRODUCTION

Micro-channels are fabricated by various methods and used in integrated circuits, micro-sensors, and micro total chemical analysis systems (μ-TAS), among others, with the objective of heat exchange or emission, delivery of liquid or gas between fluidic components, diffusion, and so on. The fabrication methods for micro-channels are mostly based on microelectromechanical system (MEMS) technology. One of these methods is bulk micromachining in which a closed micro-channel can be fabricated by bonding an etched channel on a substrate with a regular substrate as a lid [1], by sealing an etched channel with deposition of LPCVD oxide or others [2], or by

seeding and growing a diamond on an etched silicon substrate using deep-reactive ion etching (Deep RIE) [3]. In bulk micromachining, additional processes such as bonding or sealing after producing the open channel and a clean room are sometimes needed [4], and these result in cost increases and additional process complexity. The size of the micro-channel using these methods are from several microns to a few hundred microns and the shape is limited to 2 dimensions such as a rectangle because of the nature of the process.

Using another MEMS process called surface micromachining, various micro-channels have been fabricated [5-8]. This process also leads to additional costs associated with using a clean room and manufacturing of a physical mask. With the combination of surface micromachining and other techniques, a micro-channel fabrication method using SU-8, which is a thick-film photo-plastic, was suggested [9]. Chuang *et al.* [10] fabricated a multi-layer embedded micro-channel by controlling UV dosage and anti-reflection coating on a bottom surface. Tay *et al.* [11] suggested direct write of a proton beam on SU-8 to make a micro-channel. While these methods are relatively simple, they require an additional bonding process with electronics. Even though the achievable size is as small as a few microns, the cross-section of the fabricated micro-channels is again limited to 2 dimensions.

In another example, a high aspect ratio vertical micro-channel was fabricated using the LIGA process, where LIGA represents a German acronym for a manufacturing process that includes lithography, electro-forming, and molding. Although LIGA can produce highly detailed micro-features, there are a number of limitations on horizontal channel fabrication [12]. Lee *et al.* [13] fabricated a micro-channel for an inkjet head by combination of MEMS technology and a Ni electroplating process. Mizuno *et al.* [14] suggested a fabrication method with hot emboss and poly(methyl methacrylate) (PMMA) materials. In this process, a silicon wafer was first etched, a PMMA plate with an open channel was generated by hot emboss, and a closed channel was fabricated by bonding a PMMA pen channel with a regular PMMA plate. Mizukami *et al.* [15] fabricated a micro-channel with a smooth surface without a bonding process using the SD method, which is referred to as "Stereolithography with Double controlled surface." Hawkins *et al.* fabricated an adhesiveless microfluidic device using solvent assisted thermal welding, where polymer films were used as the material (Mylar sheets), and these sheets were cut and combined according to the fluidic design [16].

There are several methods to produce circular cross-section micro-channels using soft materials. Verma *et al.* [17] fabricated a polydimethylsiloxane (PDMS) micro-channel by molding PDMS around a nylon thread and pulling out the thread from the mold, leaving a micro-channel. Using this method, Verma *et al.* fabricated various complex 3D micro-channels with diameters of ~50 μm to ~250 μm. Golden and Tien [18] fabricated microfluidic hydrogels to be used in tissue engineering applications using molded gelatin as a sacrificial layer, where a micro-

channel was as narrow as ~6 μm. Though these methods are promising in 3D complex micro-channel fabrication, they cannot produce solid micro-channels because of the nature of the processes and materials. In addition, several studies have demonstrated the fabrication of a micro-channel using a microstereolithography system, which evolved from conventional stereolithography [19, 20]. Using this technology, a biomedical integrated chip (IC) [21], a micro-mixer [22], a micro-ABO blood typing system [23], and artificial human vessels [24] were successfully produced. Using this technology, the micro-channel on a large area over a few cm cannot be easily produced because the systems are focused on producing objects with the range of just a few mm.

Even though many methods to produce micro-channels have been developed, these methods have yet to produce long horizontal micro-channels with circular cross-section on the order of tens of microns and contained within a moderately solid and robust package. In our previous research [25], vertical and horizontal micro-channel fabrication using commercial line-scan stereolithography (SL) was suggested. In line-scan SL, the ability to fabricate vertical micro-channels depends primarily on the spot size of the focused laser, but for horizontal micro-channels, successful fabrication depends on the spot size, cure depth, layer thickness, and possibly other factors. The cure depth (or the depth of penetration of the laser beam into the photocurable resin) mostly affects the geometry of the down-facing surface, and it is this characteristic of SL that makes horizontal micro-channel fabrication extremely difficult. That is, what typically happens when building the down-facing surface of a micro-channel is the laser will simply penetrate into the micro-channel completely crosslinking the resin within the channel, and thus entirely eliminating the intended micro-channel. As a result, SL has not previously been considered as a reliable method for fabricating horizontal embedded micro-channels.

In this paper, a method for successful fabrication of horizontal micro-channels using commercial line-scan SL has been developed that involves first building an open micro-channel, interrupting the SL process and inserting a micro-wire, and then capping over the wire with multiple layers. After a part with the micro-wire was successfully fabricated, the part was post-cured for a certain time to cure any unreacted resin around the wire. Once post-cured, the micro-channel was obtained by removing the micro-wire from the fabricated part. To demonstrate the ability of this simple and inexpensive process to fabricate these channels, a method for inserting the wire during fabrication was developed that also included the design of a fixture. In the current research, three different wire diameters were used and tested. SEM images were obtained to examine the geometries of the micro-channels, and the diameters of the micro-channels along the build and scan directions were measured. A statistical design of experiments using measured data was performed to show that the process was capable of

producing accurate horizontal micro-channels. The following sections contain more details of the methods and results obtained from this research.

MATERIALS AND METHODS

Materials

Micro-wire with nominal diameters of 27.9 μm (0.0011 inch), 53.3 μm (0.0021 inch), and 78.7 μm (0.0031 inch) were provided from Phoenix Wire Inc. (South Hero, Vermont). The micro-wires were coated with 2.5 μm (0.0001 inch) thick Teflon using bare wires of 25.4 μm (0.001 inch), 50.8 μm (0.002 inch), and 76.2 μm(0.003 inch) diameters, respectively. The nominal dimensions were provided from the manufacturer, and the actual individual wire dimensions were measured as will be discussed later. The three coated micro-wire sizes will be referred to as mw1, mw2, and mw3 for convenience. Micro-channel specimens were fabricated using a Viper si2^{TM} SL system (3D Systems Inc.) and DSM Somos® WaterShed^{TM} 11120 resin.

Fixture model

To more easily fabricate micro-channel specimens and handle the wire, a fixture was designed as shown in Fig. 1. The fixture included aligning and tying posts on each side of the specimen, where each post was used to secure the wire on each end of the specimen. Each end of the wire was wrapped around an aligning post and secured by tying to a tying post. The fixture was designed for seven specimens where each specimen was built on top of a base plate. Each specimen had guidance grooves built into the fixture for wire alignment. The tying posts were also capped with ring fasteners that were used for wire tensioning.

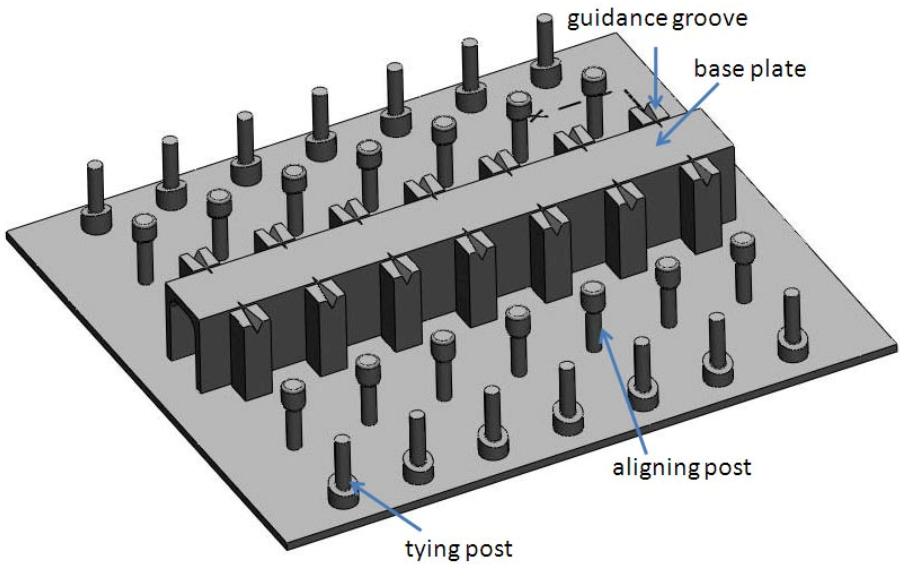

Fig. 1 Wire embedding fixture

Specimen model

The specimens consisted of 4 types of layers as shown in Fig. 2. Fig. 2 (a) and (b) were used for base layers with the thickness of 2.2352 mm, Fig. 2 (c) was used for the open channel with the width of 0.1016 mm and the thickness of 0.1524 mm (3 layers), and Fig. 2 (d) was used for capping layers with the thickness of 0.254 mm (5 layers), where the stacking layer thickness was used as 50.8 μm (0.002 inch) in high resolution mode in the machine. Fig. 3 shows the 3D model of the specimens with the size of 10 mm × 12 mm × 2.489 mm, where the wedge groove was used to assist with breaking the specimens into two parts in order to inspect the inside of the fabricated micro-channel.

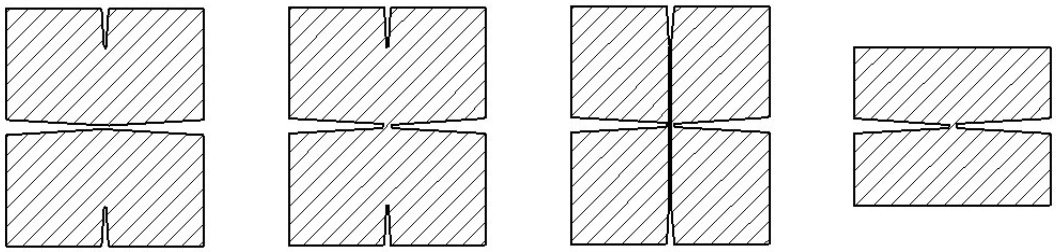

(a) (b) (c) (d)

Fig. 2 Sliced layers for the specimens: (a) bottom layers, (b) intermediate layers, (c) open channel layers, and (d) capping layers

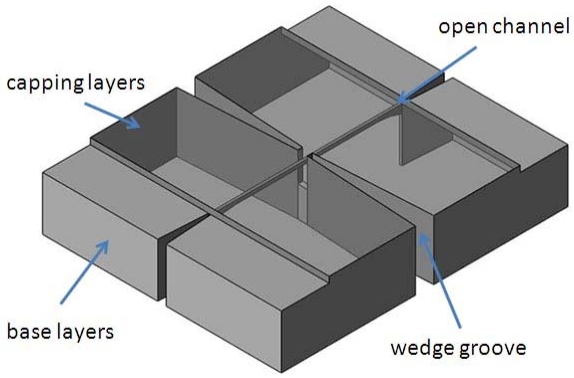

Fig. 3 Specimen model

Micro-channel fabrication

After fabricating the fixture, a Mylar sheet was put on top of the base plate to act as the specimen build platform so that the specimens could be built without base support and the fixture could be reused as needed. The micro-channel specimen was built on the Mylar sheet by fabricating an open channel in the specimen (Fig. 4 (a)), inserting the micro-wire within the open channel (Fig.

4 (b)) while interrupting the machine, capping over the micro-wire with the designed capping layers (Fig. 4 (c)), removing the specimen from the fixture after cutting the ends of the micro-wires (releasing the wires from the posts), rinsing the sample with isopropyl alcohol (IPA), post-curing for ~30 min on each side, and pulling the micro-wire out of the specimen (Fig. 4 (d)). For precisely embedding micro-wires on the open channel, one of the ends of micro-wire was tied at the tying post, and it was aligned using the aligning post and the wedge guidance groove. To maintain wire tension during the insertion process, the other end of the micro-wire was tied at the other tying post as the wire was manually inserted into the open channel. Once inserted and capped, each specimen was post-cured in order to completely solidify uncured resin around the embedded micro-wire. To remove the wire, one end of micro-wire was picked up with a tool (needle nose pliers), and the wire was manually and slowly removed from the specimen. This process is simple and straightforward, although considerable development was required to develop the final process described here. Much of the preliminary wire embedding research from which the current work is based can be found in Ranade [27].

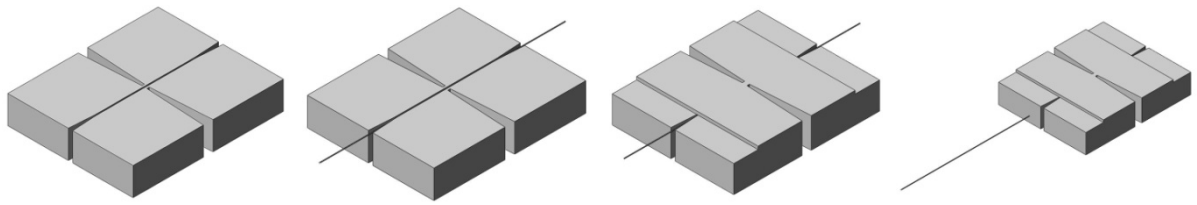

(a) (b) (c) (d)

Fig. 4 The process for micro-channel fabrication: (a) fabrication of open channel, (b) embedding the micro-wire, (c) capping, and (d) pulling the micro-wire

Metrology

To verify that the fabricated micro-channel exists with the circular shape in the specimen, the inside of the specimen has to be inspected. The specimen was designed to be easily broken by the wedge groove as shown in Fig. 3. After removing the micro-wire, the specimen was split into two parts as shown in Fig. 5 (a). To inspect the micro-channel, a scanning electron microscope (SEM) was used and each end of the split part was inspected as shown in Fig. 5 (b). The micro-channel was measured along the build direction and scan direction as shown in Fig. 5 (b) and these measurements were recorded. For statistical analysis, four builds consisting of five specimens each were fabricated for each of three different size micro-wires. All specimens in each build were randomly inspected using the SEM.

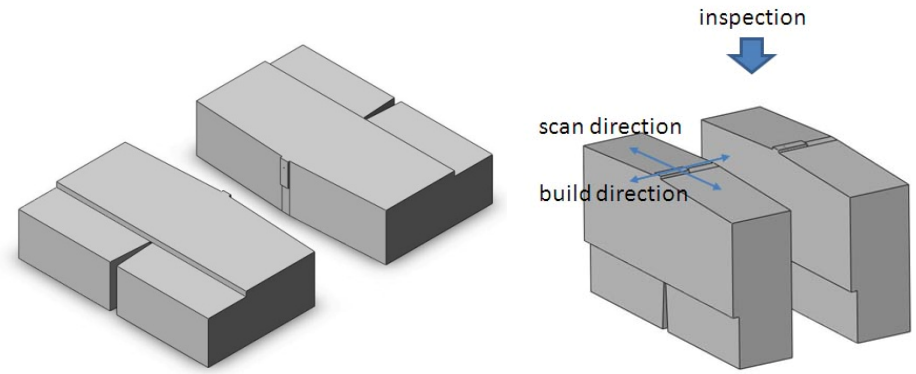

(a) (b)

Fig. 5 Broken specimen for inspection: (a) broken specimen, and (b) specimen setting for inspection

MICRO-CHANNEL FABRICATION AND INSPECTION

Micro-channel fabrication

The fabricated fixture and specimen are shown in Fig. 6 (a), and the embedded micro-wire with the fabricated specimen is shown in Fig. 6 (b). After embedding the micro-wire, capping over the micro-wire, and cutting the micro-wire, the specimens on the Mylar sheet were removed as shown in Fig. 7. These specimens were rinsed with the IPA, and post-cured for ~30 min on each side. Fig. 8 shows post-cured specimens with the micro-wires, and the micro-wire was pulled out of the specimen as shown in Fig. 9 (a). To measure the inside of the micro-channel the post-cured specimens were split into two parts as shown in Fig. 9 (b).

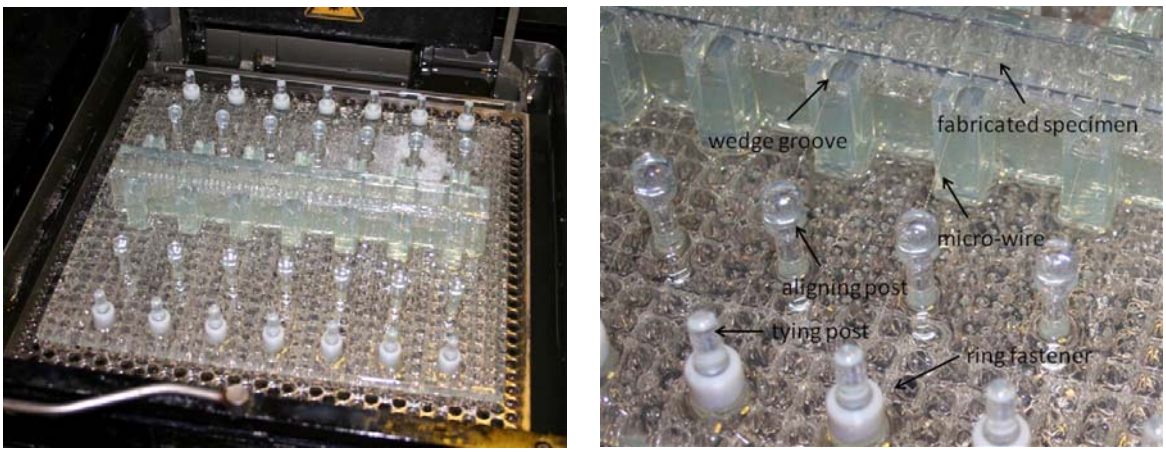

(a) (b)

Fig. 6 Fixture and specimen: (a) fabricated fixture and specimen in the machine, (b) magnified image of the fixture and specimen

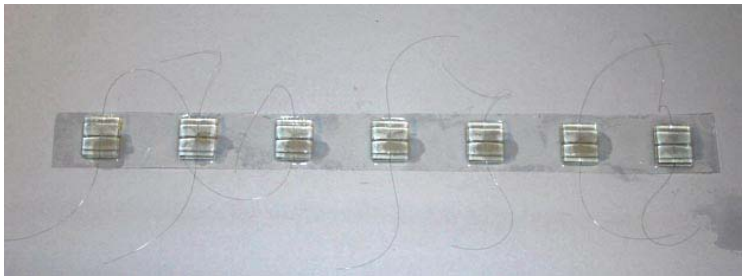

Fig. 7 Fabricated specimens on the Mylar sheet

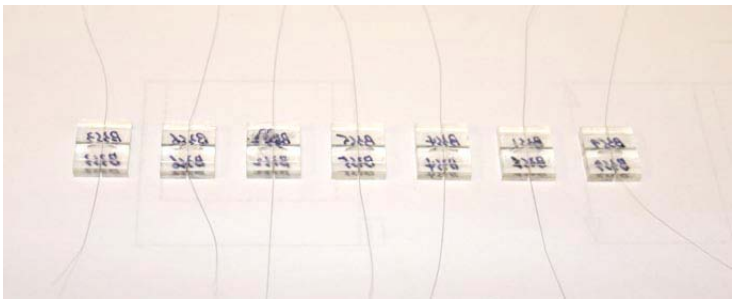

Fig. 8 Specimens after post-curing

(a)

(b)

Fig. 9 Specimens after pulling the micro-wire: (a) specimens, (b) broken specimens

Micro-wire measurement

The diameters of the bare wires (Fig. 10) and coated wires (Fig. 11) were measured for comparison with the reported nominal diameters. The measured diameters of the bare wires were 28.2 μm, 54.2 μm, and 78.1 μm, respectively, which are larger than the nominal wire diameters of 25.4 μm, 50.8 μm, and 76.2 μm, respectively. The coated wires (Fig. 11) were also larger than their reported values: 31.6 μm for the 27.9 μm (0.0011 inch) wire, 57.2 μm for the 53.3 μm (0.0021 inch) wire, and 83.5 μm for the 78.7 μm (0.0031 inch) wire. Based on the measured values, the approximate Teflon coating thicknesses are 3.5 μm, 3.1 μm, and 5.4 μm, respectively.

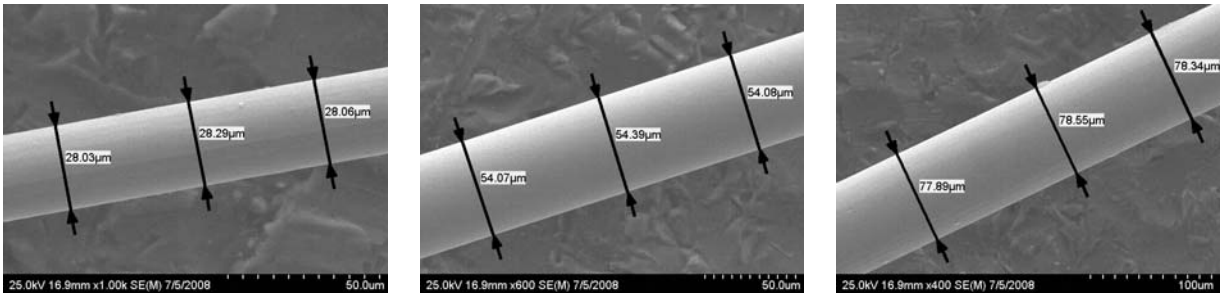

(a) (b) (c)

Fig. 10 SEM images of bare micro-wires: (a) 25.4 µm, (b) 50.8 µm, and (c) 76.2 µm wire

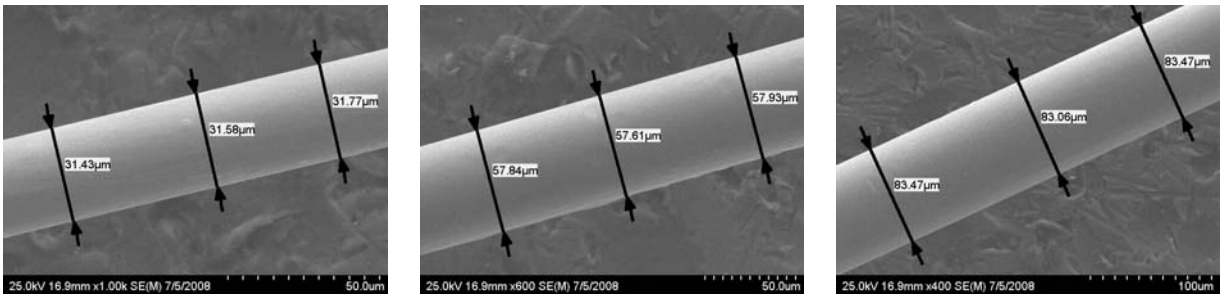

(a) (b) (c)

Fig. 11 SEM images of Teflon coated micro-wires: (a) mw1 (b) mw2, and (c) mw3

Micro-channel metrology

Using the method to produce the micro-channel described above, circular micro-channels were successfully fabricated as shown in Fig. 12 for wires of three different diameters (31.6 µm, 57.2 µm, and 83.5 µm wire). To measure the diameters of the micro-channel, the inside of the circular channel was measured along the scan direction (horizontal direction), and build direction (vertical direction). The results demonstrate that the method described here can be used to fabricate precise micro-channels with circular cross-section.

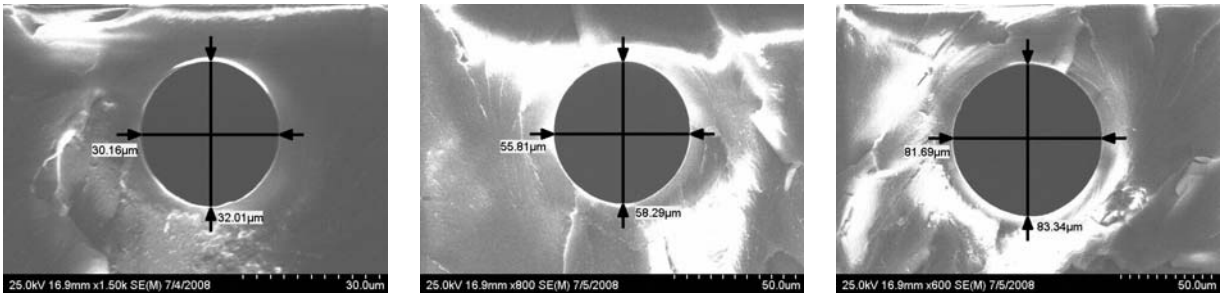

(a) (b) (c)

Fig. 12 SEM images of micro-channel: (a) mw1, (b) mw2, and (c) mw3

STATISTICAL ANALYSIS

The following describes and provides rationale for the experimental design and presents the experimental results and concomitant statistical analysis. The key assumptions underlying the adequacy of the statistical models are then presented. The completely randomized factorial experiment on the fabricated micro channels involved the study of the effects of four factors (Build, Specimen, Diameter or initial mean wire diameter, and Orientation – X and Y measured channel diameter) on the difference between the Diameter and the measured diameter of the fabricated micro channel (herein referred to as Diff). This preliminary investigation was focused on determining what effects the factors have on the diameter of the fabricated micro channel.

In each complete replication of the experiment, all possible combinations of the levels of the factors (4 for Build, 5 for Specimen, 3 for Diameter and 2 for Orientation) were investigated. All 60 parts were made from the material batch from the same manufacturer. Therefore, a four-factor factorial model was developed, using Build, Specimen, Diameter and Orientation as factors with Diff as the dependent variable. The four-factor analysis of variance model is provided in Eq. 1.

$$\begin{aligned} y_{ijkl} = {} & \mu + \tau_i + \beta_j + \gamma_k + \chi_l + (\tau\beta)_{ij} + (\tau\gamma)_{ik} + (\tau\chi)_{il} + (\beta\gamma)_{jk} + (\beta\chi)_{jl} + \\ & (\tau\beta\gamma)_{ijk} + (\tau\beta\chi)_{ijl} + (\beta\gamma\chi)_{jkl} + (\tau\beta\gamma\chi)_{ijkl} + \\ & \varepsilon_{ijklm} \begin{cases} i = 1,2,3,4 \\ j = 1,2,3,4,5 \\ k = 1,2,3 \\ l = 1,2 \\ m = 1 \end{cases} \end{aligned} \tag{1}$$

where τ represents the Build factor with 4 levels, β the Specimen factor with 5 levels, γ the Diameter factor with 3 levels (31.6 μm, 57.2 μm and 83.5 μm) and χ the Orientation factor with 2 levels (X dimension = 1 and Y dimension = 2) constituting 120 complete cases (5 × 4 × 3 × 2) made in random order. Note that ε, the random error component, has a single level corresponding to a single replicate per cell.

Experimental results

Table 1 shows the individual specimen measurements for all of the samples used in the statistical analysis. Several observations can be made based upon the experimental results contained in table 1. First, the overall average micro-channel diameters for each of the three diameters are

consistently smaller than the diameter of the embedded wires themselves (except for the measured Y diameter for the 57.2 μm wire). This is a curious result requiring additional investigation, although the maximum diameter difference is no more than 2.7 μm, which may result from deformation of the Teflon coating on the wire during fabrication. There are several other possibilities for this difference and we are currently investigation this issue. Second, the measured channel diameter in the build direction (Y Diameter) is consistently greater than the diameter in the scan direction (X Diameter). The maximum difference between the X and Y diameters is 4.6 μm and more regularly on the order of 1 μm. This too is a curious result that is requiring additional investigation.

Table 1 Results showing experimental data from SEM measurements of X and Y channel diameters for 4 Builds with 5 Specimens each.

		mw1 (Diameter 31.6 μm)		mw2 (Diameter 57.2 μm)		mw3 (Diameter 83.5 μm)	
Build	Specimen	X Dia. (μm)	Y Dia. (μm)	X Dia. (μm)	Y Dia. (μm)	X Dia. (μm)	Y Dia. (μm)
1	1	29.77	32.94	55.07	58.54	81.03	80.04
	2	29.57	30.76	55.07	58.04	82.35	80.37
	3	30.36	31.35	55.07	59.28	79.04	81.69
	4	29.96	29.77	57.79	58.29	79.04	81.03
	5	30.56	30.96	56.8	58.79	83.01	83.68
	Average	**30.044**	**31.156**	**55.96**	**58.588**	**80.894**	**81.362**
2	1	29.57	30.36	55.81	59.53	80.7	82.35
	2	30.36	32.35	55.31	60.28	81.03	85
	3	28.97	30.56	55.81	60.28	80.04	82.68
	4	28.58	30.36	55.31	58.54	81.69	83.34
	5	29.17	30.76	55.56	62.01	81.36	83.68
	Average	**29.33**	**30.878**	**55.56**	**60.128**	**80.964**	**83.41**
3	1	28.97	31.15	55.31	57.55	79.38	83.34
	2	30.36	31.95	56.06	58.04	77.06	84.67
	3	28.38	29.77	54.82	58.79	82.02	82.02
	4	29.17	30.56	56.06	58.04	81.03	85.99
	5	28.97	30.76	56.31	58.29	80.37	84.34
	Average	**29.17**	**30.838**	**55.712**	**58.142**	**79.972**	**84.072**
4	1	29.96	31.95	55.81	58.79	81.03	81.69
	2	30.16	32.15	55.31	61.27	79.71	82.68
	3	30.16	31.75	57.79	56.06	81.69	82.02
	4	29.37	31.55	56.31	60.03	82.68	81.69
	5	29.37	31.35	57.55	58.79	82.02	83.01
	Average	**29.804**	**31.75**	**56.554**	**58.988**	**81.426**	**82.218**
Overall Average		**29.587**	**31.1555**	**55.9465**	**58.9615**	**80.814**	**82.7655**
Overall St. Dev.		**0.62302568**	**0.82973173**	**0.88843275**	**1.30382236**	**1.41532823**	**1.49727578**

Table 2 shows the mean Diff for each level of the factors. It also shows the standard error of each mean, which is a measure of its sampling variability. The rightmost two columns show 95.0% confidence intervals for each of the means. Fig. 13 depicts these results graphically. Note that only the Diameter factor shows clear differences between all of its levels. This key finding is determined analytically in the next section.

Multifactor analysis

A multifactor Analysis of Variance (ANOVA) for the dependent variable Diff by levels of the Build, Specimen, Diameter and Orientation factors is first presented. Various tests and graphs to determine which factors have a statistically significant effect on the dependent variables were performed, as well as tests for significant interactions amongst the factors.

The multifactor ANOVA, summarized in Table 3, decomposes the variability of the dependent variable into contributions due to the various factors [26]. All F-ratios are based on the residual mean square error. Further, Type III sums of squares was utilized since it allows for the contribution of each factor to be measured after having removed the effects of all other factors.

Table 2 Least squares means for Diff with 95.0 percent confidence intervals

Level	Count	Mean	Standard Error	Lower Limit	Upper Limit
Grand Mean	120	-0.895			
Build 1	30	-0.109933	0.216653	-1.52873	-0.669934
Build 2	30	-0.721667	0.216653	-1.15107	-0.292267
Build 3	30	-1.11567	0.216653	-1.54507	-0.686267
Build 4	30	-0.643333	0.216653	-1.07273	-0.213934
Diameter 31.6	40	-1.22875	0.187627	-1.60062	-0.856879
Diameter 57.2	40	0.254	0.187627	-0.117871	0.625871
Diameter 83.5	40	-1.71025	0.187627	-2.08212	-1.33838
Orientation 1	60	-1.98417	0.153197	-2.2878	-1.68054
Orientation 2	60	0.194167	0.153197	-0.109465	0.497798
Specimen 1	24	-1.15667	0.242225	-1.63675	-0.676583
Specimen 2	24	-0.770417	0.242225	-1.2505	-0.290333
Specimen 3	24	-1.16667	0.242225	-1.64675	-0.686583
Specimen 4	24	-0.925833	0.242225	-1.40592	-0.44575
Specimen 5	24	-0.455417	0.242225	-0.9355	0.0246668

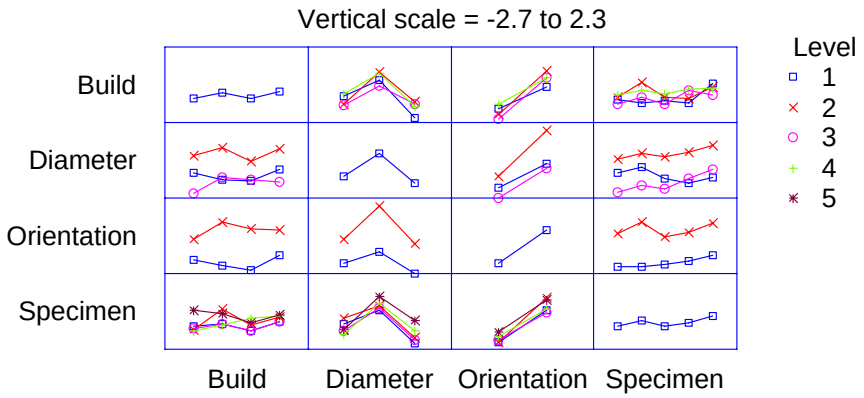

Fig. 13 Factor means plot for Diff

Table 3 Analysis of variance for Diff – Type III sums of squares

	Source	Sum of Squares	Df	Mean Square	F-Ratio	P-Value
Main Effects	**A: Build**	5.51479	3	1.83826	1.31	0.2764
	B: Diameter	83.8489	2	41.9245	29.77	0.0000
	C: Orientation	142.354	1	142.354	101.09	0.0000
	D: Specimen	8.44746	4	2.11186	1.50	0.2073
Residual		153.489	109	1.40815		
Total (Corrected)		393.654	119			

* All F-ratios are based on the residual mean square error.

The above analysis indicates that Diameter and Orientation, with p-values ~0, are the only factors that have a significant effect on Diff. Tables 4 and 5 apply a multiple comparison procedure to determine which means are significantly different from which others for Diff by the significant factors Diameter and Orientation. The bottom half of the output shows the estimated difference between each pair of means. Within each column, the levels containing X's form a group of means within which there are no statistically significant differences. The method used to discriminate among the means is Fisher's least significant difference (LSD) procedure. With this method, there is a 5.0% risk of calling each pair of means significantly different when the actual difference equals 0 [26].

Table 4 Multiple range tests for Diff by Diameter

Method: 95.0 percent LSD

Diameter	Count	LS Mean	LS Sigme	Homogeneous Groups
83.5	40	-1.71025	0.187627	X
31.6	40	-1.22875	0.187627	X
57.2	40	0.254	0.187627	X

Contrast	Difference	± Limits
31.6-57.2	*-1.48275	0.525905
31.6-83.5	0.4815	0.525905
57.2-83.5	*1.96425	0.525905

* denotes a statistically significant difference.

Table 5 Multiple range tests for Diff by Orientation

Method: 95.0 percent LSD

Orientation	Count	LS Mean	LS Sigma	Homogeneous Groups
1	60	-1.98417	0.153197	X
2	60	0.194167	0.153197	X

Contrast	Difference	± Limits
1-2	*-2.17833	0.4294

* denotes a statistically significant difference.

The following summarizes these findings:

- Since the p-values for Build and Specimen were greater than .05, we conclude that these factors have no effect on Diff at the 95% confidence level. However, differences between 2 contrasts in Specimen with respect to Diff were found, shown in Fig. 14.
- There are statistically significant differences between the mean values of Diff from one level of Diameter and Orientation (shown by an asterisk next to the pairs in the preceding tables), respectively, to another at a level of confidence of 95%, as depicted in Fig. 15 and 16.

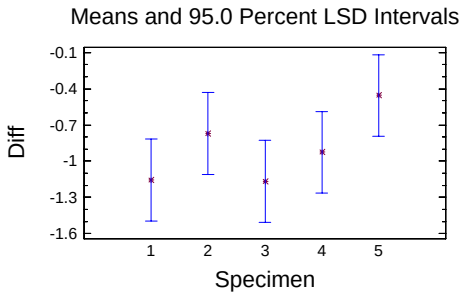

Fig. 14 means and 95 % LSD intervals between levels of Specimen and Diff

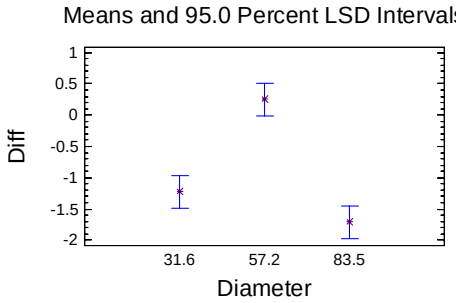

Fig. 15 Means and 95 % LSD intervals between levels of Diameter and Diff

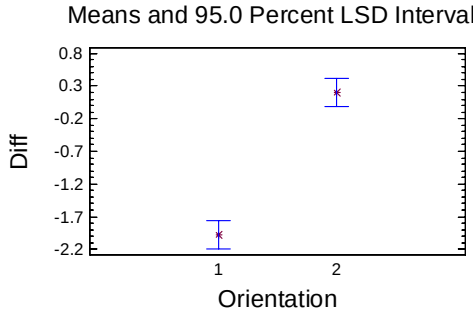

Fig. 16 and 95 % LSD intervals between levels of Orientation and Diff

Table 6 summarizes the significance of factor levels versus Diff at a level of confidence of 95.0 %. Recall that Diameter and Orientation were the only factors that had a statistically significant effect on the dependent variable Diff at the 95.0 % level of confidence. As expected, the diameter of the embedded wire has a statistically significant effect on the resulting channel diameter. However, what is less obvious is the significance of Orientation on the micro-channel diameter. As noted in the discussion for Table 1, the measured channel diameter in the build direction (Y Diameter) is consistently greater than the diameter in the scan direction (X Diameter). The maximum difference between the X and Y diameters is 4.6 μm but is more

typically on the order of 1 μm. The explanation for this result is requiring additional investigation.

Table 6 Significance summary of Diff by factor at the 95 % level of confidence

Factor		Build				Specimen					Diameter			Orientation	
	Level	1	2	3	4	1	2	3	4	5	1	2	3	1	2
Build	1														
	2														
	3														
	4														
Specimen	1									*					
	2														
	3									*					
	4														
	5					*		*							
Diameter	1											*			
	2										*		*		
	3											*			
Orientation	1														*
	2													*	

Finally, Table 7 shows the analysis of variance table which divides the variance of Diff into 4 components, one for each factor, in order to estimate the amount of variability contributed by each of the factors (variance components). Each factor after the first is nested in the one above. In this case, the factor contributing the most variance is Orientation. Its contribution represents 71.22% of the total variation in Diff. The effect of Orientation is seemingly very important and has become a focus of current investigations.

Table 7 Analysis of Variance for Diff

Source	Sum of Squares	Df	Mean Square	Var. Comp.	Percent
Total (Corrected)	393.654	119			
Build	5.51479	3	1.83826	0.0	0.00
Diameter	94.7008	8	11.8376	0.0	0.00
Orientation	183.609	12	15.3007	2.83133	71.22
Specimen	109.83	96	1.14406	1.14406	28.78

Model adequacy

In all models generated, no indications were present to assume that the fundamental conditions for the models were violated, based on the following analyses:

- The normal probability plots do not reveal violations of the normal and identically distributed (NID) error term.
- The residuals are structureless; that is, the plot of residuals versus fitted values of the dependent variables did not reveal any obvious patterns.
- Standardized residuals were approximately normal with mean = 0 and unit variance – no residual was greater than 2 standard deviations, and thus outliers did not seriously distort the ANOVA.
- The residual plots showed no significant tendencies, and thus no correlation between residuals.
- No 2-factor interactions in the models were present.
- The assumption that the variance of the observations did not change significantly as the magnitude of the observation changed is upheld utilizing Cochran's C, Hartley's and Levene's tests [26]. It should be noted that the measuring instruments were calibrated before each test.

CONCLUSIONS

A method for fabricating circular micro-channels with diameters of a few tens microns was developed using commercial line-scan stereolithography, and this method was demonstrated using a 3D Systems Viper si2^{TM} SL system and DSM Somos$^{®}$ WaterShed^{TM} resin. The method consisted of inserting a wire of specified diameter during the build, building around the inserted wire, and removing the wire once fabricated leaving a channel with a circular cross-sectional geometry equivalent to the wire diameter. Teflon coated micro-wires of diameters 31.6 μm, 57.2 μm and 83.5 μm were used and a fixture was designed to provide for easy wire handling and fabrication of multiple specimens. The fabricated specimens were split into two parts to inspect the inside of the micro-channels, and the micro-channel diameters were measured using an SEM. The measured data showed that the micro-wire was successfully removed from the channel, leaving high quality micro-channels with diameters similar to the embedded wire. A statistical analysis was conducted, and it is concluded that the suggested process is capable of producing horizontal circular micro-channels with diameters that vary with the embedded wire diameter. However, the statistical analysis also found that the diameter of the micro-channel was statistically different depending on whether it was measured in the scan direction or build direction. This result was unexpected and we are currently investigating possible sources for these differences. In conclusion, because this process is simple and fast, we believe line-scan

stereolithography can be used to produce a wide variety of unique micro-fluidic and other micro-channel devices.

ACKNOWLEDGMENTS

The facilities within the W.M. Keck Center for 3D Innovation (Keck Center) used here contain equipment purchased through Grant Number 11804 from the W.M. Keck Foundation, a faculty STARS Award and two equipment grants from the University of Texas System, and two equipment grants from Sandia National Laboratories. Frank Medina, Keck Center Manager, designed the original wire embedding fixture from which much of this work was based, trained JWC on how to embed wires during stereolithography fabrication, and assisted in various ways during this research, and his efforts are appreciated. The SEM images were acquired using an SEM funded through NSF grant DMR-0521650. This material is based in part upon work supported through the Mr. and Mrs. MacIntosh Murchison Chair I in Engineering, research contract 504004 from Sandia National Laboratories in the Laboratory Directed Research and Development (LDRD) program, and a research contract from the U.S. Army Space and Missile Defense Command and the Homeland Protection Institute to the UTEP Center for Defense Systems Research. Sandia National Laboratories is a multi-program laboratory operated by Sandia Corporation, a Lockheed Martin Company, for the United States Department of Energy's National Nuclear Security Administration under contract DE-AC04-94AL85000. The findings and opinions presented in this paper are those of the authors and do not necessarily reflect those of the sponsors of this research.

REFERENCES

[1] Nakanishi H., Nishimoto T., Nakamura N., Nagamachi S., Arai A., Iwata Y., and Mito Y., "Fabrication of electrophoresis devices on quartz and glass substrates using a bonding with HF solution," *in Proc. IEEE MEMS'97*, Nagoya, Japan, Jan. 26-30, 1997, pp. 299~304.

[2] Kaplan W., Elderstig H., and Vieider C., "A novel fabrication method of capillary tubes on quartz for chemical analysis application," *in Proc. IEEE MEMS'94*, Int. Conf. MEMS, Oiso, Japan, Jan. 25-28, 1994, pp. 63~68.

[3] Guillaudeu S., Zhu X., Aslam D.M., "Fabrication of 2-um wide poly-crystalline diamond channels using silicon molds for micro-fluidic applications," *Diamond and Related Materials*, Vol. 12, 2003, pp. 65~69.

[4] Rasmussen A., Gaitan M., Locascio L.E., and Zaghloul M.E., "Fabrication Techniques to Realize CMOS-Compatible Microfluidic Microchannels," *Journal of Microelectromechanical Systems*, Vol. 10, No. 2, 2001, pp. 286~297.

[5] Chen J., and Wise K.D., "A High-resolution silicon monolithic nozzle array for inkjet printing," *The 8th Int. Conf. on Solid-State Sensors and Actuators, and Eurosensors IX,* Stockholm, Sweden, June 25-29, 1995, pp. 321~324.
[6] Liu C.W., Gau C., and Dai B.T., "Design and fabrication development of a micro flow heated channel with measurements of the inside micro-scale flow and heat transfer process," *Biosensors and Bioelectronics*, Vol. 20, 2004, pp. 91~101.
[7] Liu C.W., Gau C., Ko H.S., Yang C.S., and Dai B.T., "Fabrication challenges for a complicated micro-flow channel system at low temperature process," *Sensors and Actuators A* 130-131, 2006, pp. 575~582.
[8] Ko H.S., Liu C.W., Gau C., and Yang C.S., "Fabrication and design of a heat transfer micro-channel system by a low temperature MEMS technique," *Journal of Micromechanics and Microengineering*, Vol. 17, 2007, pp. 983~993.
[9] Guerin L.J., Bossel M., Demierre M., Calmes S., and Renaud P., "Simple and low cost fabrication of embedded micro-channels by using a new thick-film photoplastic," *Transducers '97 Int. Conf. on Solid-State Sensors and Actuators*, Chicago, June 16-19, 1997, pp. 1419~1421.
[10] Chuang Y.J., Tseng F.G., Cheng J.H., and Lin W.K., "A novel fabrication method of embedded micro-channels by using SU-8 thick-film photoresists," *Sensors and Actuators A*, Vol. 103, 2003, pp. 64~69.
[11] Tay F.E.H., Kan J.A., Watt F., and Choong W.O., "A novel micro-machining method for the fabrication of thick-film SU-8 embedded micro-channels," *Journal of Micromechanics Microengineering*, Vol. 11, 2001, pp. 27~32.
[12] Liu R.H., Vasile M.J., Goettert J., and Beebe D.J., "Investigation of the LIGA process to fabricate microchannel plates," *Transducers'97 Int. Conf. on Solid-State Sensors and Actuators*, Chicago, June 16-19, 1997, pp. 645~648.
[13] Lee J.D., Yoon J.B., Kim J.K., Chung H.J., Lee C.S., Lee H.D., Lee H.J., Kim C.K., and Han C.H., "A Thermal inkjet printhead with a monolithically fabricated nozzle plate and self-aligned ink feed hole," *Journal of Microelectromechanical Systems*, Vol. 8, No. 3, 1999, pp. 229~236.
[14] Mizuno J., Harada T., Glinsner T., Ishizuka M., and Edura T., "Fabrications of Micro-Channels Device by Hot emboss and Direct bonding of PMMA," *Proc. Of the 2004 Int. Conf. on MEMS*, NANO and Smart Systems(ICMENS'04).
[15] Mizukami Y., Rajniak D., Rajniak A., and Nishimura M., "A novel microchip for capillary electrophoresis with acrylic microchannel fabricated on photosensor array," *Sensors and Actuators B*, Vol. 81, 2002, pp. 202~209.

[16] Kenneth Hawkins, David Markel, Paul Yager, Matthew S. Munson, "Method of adhesiveless lamination of polymer films into microfluidic networks with high dimensional fidelity," Pub. No. US2006/0372716 A1, Dec. 7, 2006.
[17] Verma M.K.S., Majumder A., and Ghatak A., "Embedded Template-Assisted Fabrication of Complex Microchannels in PDMS and Design of a Microfluidic Adhesive," *Langmuir*, Vol. 22, 2006, pp. 10291~10295.
[18] Andrew P. Golden and Joe Tien, "Fabrication of microfluidic hydrogels using molded gelatin as a sacrificial element," Lab On a Chip, Vol. 7, pp. 720~725, 2007.
[19] Choi J.W., Ha Y.M., Lee S.H., and Choi K.H., "Design of Microstereolithography System based on Dynamic Image Projection for Fabrication of Three-Dimensional Microstructures," *Journal of Mechanical Science and Technology*, Vol. 20, No. 12, pp. 2094~2104, 2006.
[20] Choi J.W., Wicker R.B., Cho S.H., Ha C.S., and Lee S.H., "Cure depth control for complex 3D microstructure fabrication in maskless projection microstereolithography," *Rapid Prototyping Journal,* submitted.
[21] Ikuta K., Ogata T., Tsubio M., and Kojima S., "Development of Mass Productive Micro StereoLithography(Mass-IH Process)," *MEMS'96*, pp. 301~306, 1996.
[22] Bertsch A., Bernhard P., and Renaud P., "Microstereolithography : Concepts and applications," *8th IEEE International Conference on Emerging Technologies and Factory Automation*, pp.289~298, 2001.
[23] Kang H.W., Lee I.H., and Cho D.W., "Development of an Assembly-free Process Based on Virtual Environment for Fabricating 3D Microfluidic Systems Using Microstereolithography Technology," *Journal of Manufacturing Science and Engineering*, Vol. 126, pp. 766~771, 2004.
[24] Wu D., *Micro Fabrication of 3D Structures and Characterization of Molecular Machine*, Ph.D. Dissertation, UCLA, 2005.
[25] Wicker R.B., Ranade A.V., Medina F., and Palmer J.A., "Embedded micro-channel fabrication using line-scan stereolithography," *Assembly Automation*, Vol. 25, No. 4, 2005, pp. 316~329.
[26] Montgomery D.C., *Design and Analysis of Experiments*, 5th edition, Wiley, New York, NY, 2001.
[27] Ranade A.V., *Microstereolithography of embedded micro-channels*, M.S. Thesis, University of Texas at El Paso, 2005.